

tion, the presence of degranulated mast cells in joint tissue, and not other tissues, before overt clinical or histologic inflammation supports a proximal, synovium-specific role for mast cells in the effector phase of inflammatory arthritis. Moreover, because mast cells continue to demonstrate a degranulating phenotype during more chronic phases of arthritis (Fig. 3, E to H), it is also likely they play an ongoing role in the arthritic process.

Initial results from the mast cell-deficient mouse strains left open the possibility that the SCF/c-kit signaling pathway played some role in the induction of arthritis other than via mast cells. However, the restoration of arthritis susceptibility by mast cell engraftment defined mast cells as the element that prevents disease development in SI/SI^d and W/W^v mice. The striking requirement for mast cells, coupled with evidence for their rapid degranulation within the first hours after serum transfer, leads us to suggest that mast cells may provide the cellular target of autoantibodies, the complement network, and Fc receptors in the subsequent development of inflammatory arthritis. Because C5a and FcγR ligation are potent activators of mast cell function in vitro and in vivo (16–22), it is likely that synovial mast cells are activated by articular autoantibody immune complexes suggestive of an immune complex hypersensitivity (Arthus) reaction in the synovium (23, 24).

Mast cells themselves produce a series of effector molecules that mediate permeability, inflammation, chemotaxis, and tissue destruction. They are the only cells that contain preformed TNF-α in granules and they also display an ability to rapidly produce large amounts of both TNF-α and IL-1 (25, 26), cytokines that play a critical role in K/BxN arthritis (6), as well as in human rheumatoid arthritis. Mast cell granules also contain an abundance of proteases capable of activating matrix metalloproteinases (27) and mMCP-6, a potent indirect neutrophil chemoattractant (28). These cells also produce large quantities of other inflammatory molecules including histamine, eicosanoids, fibroblast growth factor, and angiogenesis factors (VEGF), which may contribute further to the arthritic process.

Historically, mast cells have been implicated in two contrasting types of immune responses. First, they can be activated by immunoglobulin IgE receptors to mediate immediate hypersensitivity reactions associated with allergic phenomena. Second, their acute activation by microbial products, as in bacterial peritonitis models, underscores their role in infection (29, 30). Here, we present evidence of a direct role for mast cells in the pathogenesis of inflammatory arthritis. Our findings in the K/BxN model of destructive arthritis point to a likely role for mast cells in human arthritis associated with immune complex formation, namely, cryoglobulin-associated synovitis in hepatitis C infection, postinfectious arthritis, and perhaps others. Moreover, histo-

logic analyses of synovial sections from humans have documented the presence of mast cells in abundance (22) and immune complexes, complement fragments, and SCF are present in synovial fluid and tissue in rheumatoid arthritis (31–33). Together, these findings illustrate that mast cells can contribute to the pathogenic mechanisms in the synovium that result in erosive arthritis.

References and Notes

1. I. Matsumoto, A. Staub, C. Benoist, D. Mathis, *Science* **286**, 1732 (1999).
2. V. Kouskoff et al., *Cell* **87**, 811 (1996).
3. A. S. Korganow et al., *Immunity* **10**, 451 (1999).
4. B. T. Wipke, P. M. Allen, *J. Immunol.* **167**, 1601 (2001).
5. H. Ji et al., *Immunity* **16**, 157 (2002).
6. H. Ji et al., *J. Exp. Med.* **196**, 77 (2002).
7. Y. Kitamura, S. Go, K. Hatanaka, *Blood* **52**, 447 (1978).
8. Y. Kitamura et al., *J. Exp. Med.* **150**, 482 (1979).
9. C. I. Brannan et al., *Proc. Natl. Acad. Sci. U.S.A.* **88**, 4671 (1991).
10. K. M. Zsebo et al., *Cell* **63**, 213 (1990).
11. D. M. Lee et al., unpublished observations.
12. K. Nocka et al., *EMBO J.* **9**, 1805 (1990).
13. E. N. Geissler, M. A. Ryan, D. E. Housman, *Cell* **55**, 185 (1988).
14. T. Nakano et al., *J. Exp. Med.* **162**, 1025 (1985).
15. M. F. Gurish et al., *J. Exp. Med.* **175**, 1003 (1992).
16. W. Fureder et al., *J. Immunol.* **155**, 3152 (1995).

17. G. Alber, U. M. Kent, H. Metzger, *J. Immunol.* **149**, 2428 (1992).
18. H. R. Katz et al., *J. Immunol.* **148**, 868 (1992).
19. U. Baumann et al., *J. Immunol.* **164**, 1065 (2000).
20. U. Baumann et al., *J. Immunol.* **167**, 1022 (2001).
21. D. Dombrowicz et al., *J. Clin. Invest.* **99**, 915 (1997).
22. H. P. Kiener et al., *Arthritis Rheum.* **41**, 233 (1998).
23. I. Matsumoto et al., *Nature Immunol.* **3**, 360 (2002).
24. D. L. Sylvestre, J. V. Ravetch, *Immunity* **5**, 387 (1996).
25. J. R. Gordon, S. J. Galli, *Nature* **346**, 274 (1990).
26. P. R. Burd et al., *J. Exp. Med.* **170**, 245 (1989).
27. K. Suzuki, M. Lees, G. F. Newlands, H. Nagase, D. E. Woolley, *Biochem. J.* **305**, 301 (1995).
28. C. Huang et al., *J. Immunol.* **160**, 1910 (1998).
29. B. Echtenacher, D. N. Mannel, L. Hultner, *Nature* **381**, 75 (1996).
30. R. Malaviya, T. Ikeda, E. Ross, S. N. Abraham, *Nature* **381**, 77 (1996).
31. I. Broder, M. B. Urowitz, D. A. Gordon, *Med. Clin. N. Am.* **56**, 529 (1972).
32. V. E. Jones, R. K. Jacoby, P. J. Cowley, C. Warren, *Clin. Exp. Immunol.* **49**, 31 (1982).
33. M. Schaller, D. R. Burton, H. J. Ditzel, *Nature Immunol.* **2**, 746 (2001).
34. The authors gratefully acknowledge the insightful discussions and manuscript review by K. F. Austen, as well as the expert technical assistance of the histotechnicians A. Calderone, T. Bowman, D. Bowman, and L. Chen. This work was supported by NIH grant 1R01 AR/Al46580-01 (to D.M. and C.B.).

Supporting Online Material

www.sciencemag.org/cgi/content/full/297/5587/1689/DC1

Materials and Methods
Figs. S1 to S4

8 May 2002; accepted 25 July 2002

Structure, Mechanism, and Regulation of the *Neurospora* Plasma Membrane H⁺-ATPase

Werner Kühlbrandt, Johan Zeelen, Jens Dietrich*

Proton pumps in the plasma membrane of plants and yeasts maintain the intracellular pH and membrane potential. To gain insight into the molecular mechanisms of proton pumping, we built an atomic homology model of the proton pump based on the 2.6 angstrom x-ray structure of the related Ca²⁺ pump from rabbit sarcoplasmic reticulum. The model, when fitted to an 8 angstrom map of the *Neurospora* proton pump determined by electron microscopy, reveals the likely path of the proton through the membrane and shows that the nucleotide-binding domain rotates by ~70° to deliver adenosine triphosphate (ATP) to the phosphorylation site. A synthetic peptide corresponding to the carboxyl-terminal regulatory domain stimulates ATPase activity, suggesting a mechanism for proton transport regulation.

P-type ATPases are ion pumps of ~100 kD that use ATP to transport cations through the cell membrane against a concentration gradient (1). The proton ATPases in the plasma membrane of fungal and plant cells maintain the intracellular pH and membrane potential, providing energy for the uptake of nutrients and exchange of ions by

secondary transporters. The pumps cycle between the E1 and E2 states, which have different binding affinities for nucleotides and for the transported ion. A conserved aspartate (Asp³⁷⁸ in the *Neurospora* proton ATPase) is reversibly phosphorylated (1) after the proton binds to a site in the membrane from the cytoplasmic side. Phosphorylation of the aspartate results in a conformational change. This reduces affinity of the binding site for the proton that is released to the outside. Large conformational changes occurring during the pumping cycle (2, 3) were apparent from a comparison

Max-Planck-Institut für Biophysik, Heinrich-Hoffmann-Str. 7, 60528 Frankfurt am Main, Germany.

*Present address: Laboratory of Molecular Biophysics, University of Oxford, South Parks Road, Oxford OX1 3QU, UK.

REPORTS

of the structures of the sarcoplasmic Ca^{2+} -ATPase in the E1 (4) and E2 state (5) with one another and with the *Neurospora* H^{+} -ATPase (6).

Electron cryomicroscopy enabled the determination of 8 Å maps of the H^{+} -ATPase (6) and the Ca^{2+} -ATPase in the E2 state (5). These maps agreed in the arrangement of 10 transmembrane helices (designated M1 to M10) in the membrane (M) domain but indicated large differences in the cytoplasmic part. The 2.6 Å x-ray structure of the Ca^{2+} -ATPase in the E1 state (4) revealed details of the ion-binding site in the membrane and defined three cytoplasmic domains: the phosphorylation (P) domain, the nucleotide-binding (N) domain, and the A domain of unknown function.

On the basis of a detailed sequence comparison of P-type ATPases to identify conserved, functionally important regions, we built a homology model of the proton ATPase and fitted it to the 8 Å map. The alignment of the H^{+} -ATPase and Ca^{2+} -ATPase sequences is shown in fig. S1. The Ca^{2+} -ATPase has 994 residues, whereas the *Neurospora* H^{+} -ATPase has only 920, including an NH_2 -terminal extension of 67 residues and a COOH-terminal extension of 36 residues. Neither extension is present in the Ca^{2+} -ATPase. Overall, 25% of the 817 residues in the four principal domains are identical in both proteins. The homology of individual domains varies from 18% (M domain) to 39% (P domain) (table S1).

An initial comparison of the model to the map (fig. S2, A and B) indicated a very good fit of the M and P domains, whereas the N and A domains were, respectively, largely or partially outside the map density. They were fitted to the map as rigid bodies, and the NH_2 - and COOH-terminal extensions were added to the remaining, unoccupied map regions. The resulting fitted model of the proton pump is shown in Fig. 1.

The strikingly good fit of the M domain (Fig. 1, A to C) indicates that its structure is highly conserved, even though this would not be expected from the low sequence homology. The match was almost perfect for M3, M4, and M5, whereas the remaining transmembrane helices required minor

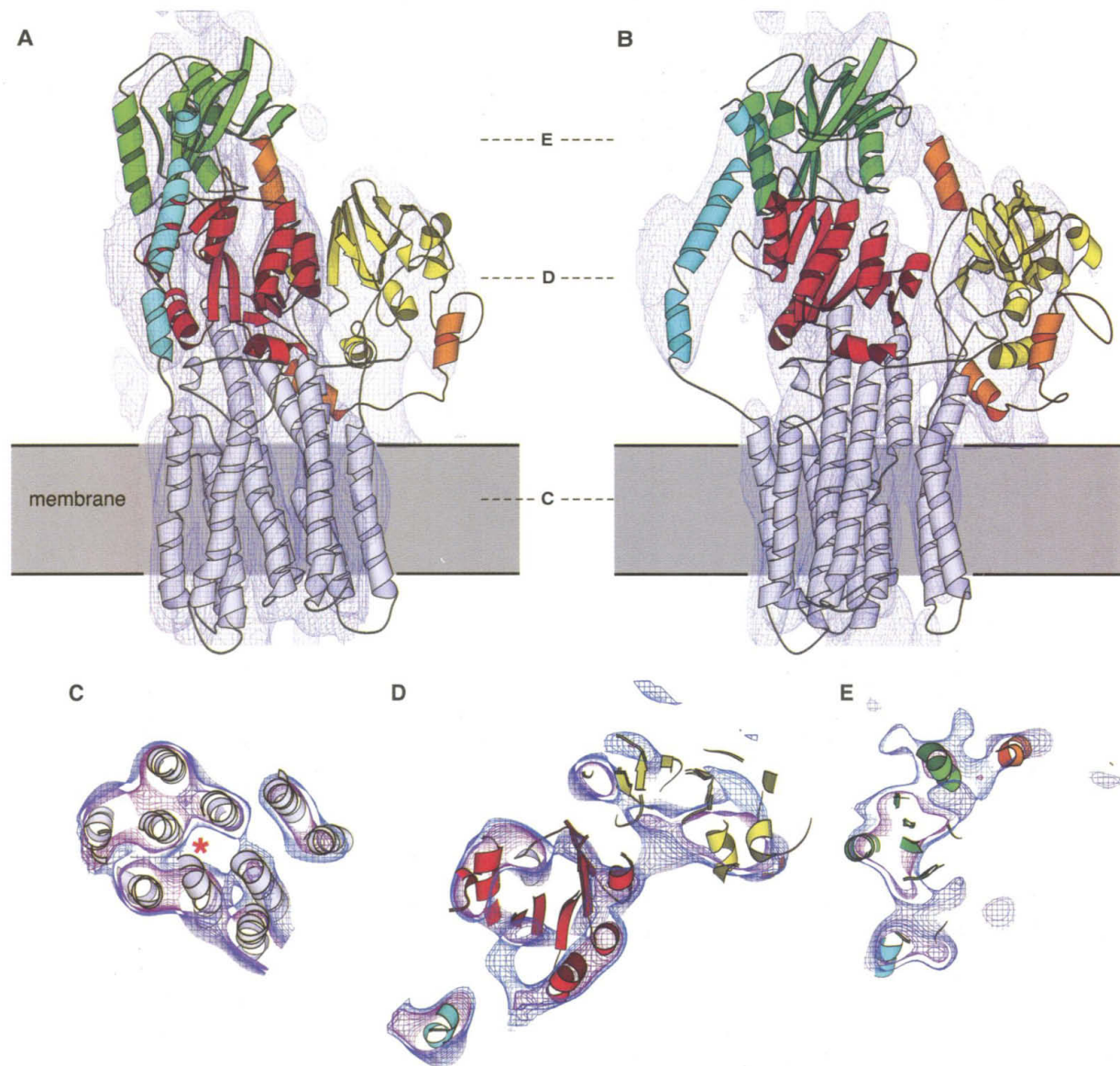


Fig. 1. Fit of the atomic model of the H^{+} -ATPase to the 8 Å map (6) (blue net). The four principal domains are shown in pink (M), red (P), green (N), and yellow (A). The COOH-terminal regulatory R domain is shown in cyan and the NH_2 -terminal extension in orange. (A) Side view. Dashed lines indicate the position of cross sections through the M, P/A, and N domains shown in (C), (D), and (E). (B) Front view. (C)

Cross section parallel to the membrane plane through the M domain. The map density in the region at the proton-binding site between helices M4, M5, M6, and M8 (red asterisk) is low. (D) Section through the P, A, and R domains. (E) Section through the N domain. The purple net in (C), (D), and (E) is drawn at a higher contour level than the blue net in (A) and (B).

REPORTS

repositioning. The root mean square (RMS) deviation of α carbons in M1 through M10 from the Ca^{2+} -ATPase structure was 2.1 Å.

The ion-binding site in the membrane is defined by Asp⁸⁰⁰ in M6 and Glu⁹⁰⁸ in M8 of the Ca^{2+} -ATPase. Both residues are highly conserved in the P-type ATPases, highlighting their importance for ion transport. In the H^{+} -ATPase, Asp⁷³⁰ and Glu⁸⁰⁵ are found in the corresponding proton-binding site. Mutagenesis data on Glu⁸⁰⁵ have not been reported, but Asp⁷³⁰ is critical for proton pumping (7). The map density in this region was conspicuously low (Fig. 1C), presumably due to the presence of water molecules near the proton-binding site. Nearby polar groups include the main-chain carbonyls of Ile³³¹, Ile³³², and Val³³⁴ in the unwound part of M4 and the side chains of Tyr⁶⁹⁴ and Ser⁶⁹⁹ in M5, which are both essential for proton pumping (7).

All other ionic and polar side chains in the Ca^{2+} -binding site (Glu⁵⁸, Glu³⁰⁹, Glu⁷⁷¹, Asn⁷⁹⁶, and Thr⁷⁹⁹) are replaced by valines or alanines in the H^{+} -ATPase. By contrast, the proton-binding site of the latter contains the basic residues Arg⁶⁹⁵ and His⁷⁰¹ (Fig. 2A). Both are completely conserved in the yeast plasma membrane proton ATPases and are essential for ATPase activity and proton pumping (7). In the plant proton pumps, His⁷⁰¹ is replaced by an arginine and Arg⁶⁹⁵ is replaced by an alanine. An arginine and two acidic side chains thus appear to be the key residues for proton transport, as in bacteriorhodopsin (8–10), another proton pump.

The conserved structure of the M domain must reflect the conserved mechanism of ion transport and a correspondingly conserved ion path. An analysis of conserved polar and ionic residues in the structures of two family members should therefore reveal those that are involved in ion conduction, especially if the proteins are not closely related, as in this case. Access to the ion-binding site from above is blocked by large, hydrophobic side chains. The E2-state model of the Ca^{2+} -ATPase (11) does not indicate a major reorientation of the helices in this region. The most likely access to the ion-binding site is therefore through a pocket of ionic and polar side chains between the cytoplasmic ends of M1 and M2. The conserved side chains of Glu¹⁰⁸ on the cytoplasmic side of M1 and Glu¹⁶² on M2 are in strategic positions for proton conduction, as are the polar side chains of Gln¹⁶¹ and Asn¹⁵⁴ in M2. Gln and Asn residues facilitate rapid proton conduction in cytochrome *f* (12) and in the bacterial reaction center (13). The low map density in this region is consistent with the presence of water molecules, as might be expected along the proton path (8–10).

The upper half of M2 is polar and is unlikely to be embedded in the lipid bilayer.

In the H^{+} -ATPase model, the cytoplasmic end of this helix is ~ 4 Å closer to M1 than in the E1 conformation of the Ca^{2+} -ATPase (4). However, in the E2 state (4), M2 is tilted toward M1 by 14° so that the two helices are close together and more or less parallel. This conformational change would block the ion path back to the cytoplasm, thus imparting a direction to the transport process. The reorientation of M2 may facilitate the 90° rotation of the A domain in the E1-E2 transition (11) because this domain is tethered to the cytoplasmic end of the helix.

The exit channel on the exocytosolic side is likely to be the shortest route from the proton-binding site to Asn⁷¹⁸ on M6, which is only 15 Å below. Asn⁷¹⁸ is at the deepest point of a shallow cavity in the exocytosolic protein surface. This cavity is wider in the H^{+} -ATPase because its exocytosolic loops are shorter than those of the Ca^{2+} -ATPase. In the H^{+} -ATPase map, a region of low density extends from Asn⁷¹⁸ to the ion-binding site, which suggests that protons may be able to leave along this path (14).

The A domain was moved sideways into the map by ~ 10 Å as a rigid body to fit the

density. Because the cytoplasmic end of M2 had moved by ~ 5 Å, the linking peptide was not strained by this repositioning. The NH_2 -terminal extension of the H^{+} -ATPase is continuous with the A domain. It was modeled on the structures of homologous sequences from two other proteins. Three short α helices, linked by extended chains (orange in Fig. 1), were fitted to the map density around three sides of the A domain, in keeping with the predominant negative charge of this extension, which requires a solvent-exposed position. The location of a major part of this acidic extension close to the membrane surface, directly above the entrance to the proton path, suggests that it acts as a pH sensor or a local proton reservoir. The local membrane potential would alter its protonation state, affecting the mobility of the A domain and of the attached M2 helix. This would be consistent with the presumed role of the NH_2 -terminal extensions of the heavy metal-pumping P-type ATPases that contain several metal-binding motifs (15), which may have an analogous function in sensing toxic heavy metal ions and in sequestering them to the channel entrance.

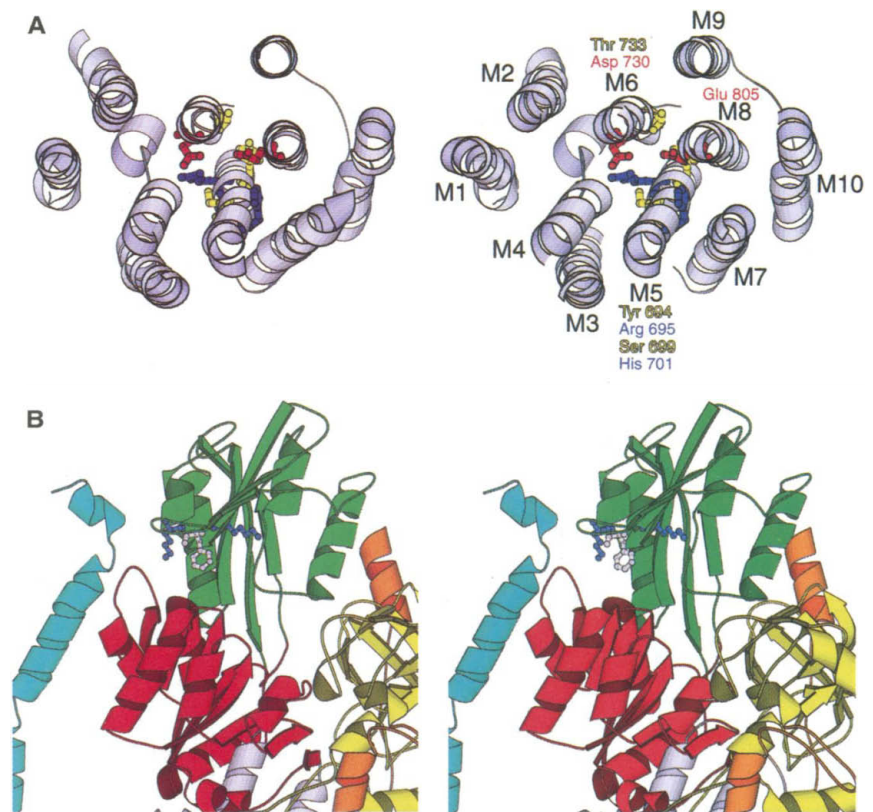


Fig. 2. Stereo diagrams of two functionally important regions of the proton ATPase. (A) The proton-binding site in the center of the M domain. Basic side chains (Arg⁶⁹⁵ and His⁷⁰¹ on M5) are blue, acidic side chains (Asp⁷³⁰ on M6, Glu⁸⁰⁵ on M8) are red, and polar side chains (Tyr⁶⁹⁴ and Ser⁶⁹⁹ on M5, Thr⁷³³ on M6) are yellow. (B) The nucleotide-binding site at the interface of the P (red), N (green), and R (cyan) domains. The side chains of residues defining the binding-site Lys⁴⁵⁶ (in front), Lys⁴⁷⁴, and Phe⁴⁵¹ are shown, with Lys in blue and Phe in pink. The model suggests that the regulatory R domain locks the N domain in position, thus rendering the ATPase inactive.

REPORTS

Most helices of the P domain Rossmann fold fitted the map density very well (Fig. 1, A, B, and D) and required only minor readjustment. Striking exceptions were the

short peripheral helices 4 and 4' (4), which were clearly outside the map density. Helix 4' required an upward tilt of $\sim 35^\circ$ around Ala⁶⁰³ to fit the map. As a result, its NH₂-terminal end came into close contact with the N domain. Excepting helices 4 and 4', the α -carbon RMS deviation from the Ca²⁺-ATPase P domain was 1.48 Å.

The N domain is connected to the P domain by two adjacent peptide strands (4). Rigid-body rotation by 73° around this hinge at Asn³⁸⁶ and Asp⁵³⁴ resulted in an optimal fit (Fig. 1, A, B, and E). As a result, Gln⁴⁶⁶ at the tip of the N domain moved by ~ 50 Å. Delivery of ATP to the phosphorylation site by tethered Brownian motion of the N domain has been proposed as a part of the Ca²⁺-ATPase mechanism (11), even though, surprisingly, the N and P domains are in nearly the same relative positions in the E1 structure and in the E2 model (11). The H⁺-ATPase model shows that the postulated movement of the N domain does indeed occur.

In the E1 state of the Ca²⁺-ATPase, the distance between the nucleotide-binding site in the N domain and the phosphorylation site in the P domain is at least 25 Å (4). In the H⁺-ATPase model, this distance is shortened to ~ 15 Å, which still seems too far for phosphate transfer. The N domain cannot move closer to the phosphorylation site without a steric clash with the

P domain (Fig. 2B), partly as a result of the reoriented helix 4', which appears to act as a doorstop for the N-domain hinge movement. Direct transfer of the phosphate to Asp³⁷⁸ would require this helix to revert to its E1 position and would also require some reorientation of the P domain.

The distance between the phosphorylation site in the P domain and the ion-binding site in the membrane is ~ 50 Å (4). The two sites are linked by M4 and M5, which contain most of the key residues in the ion-binding site. The P domain fits around the top of M5 like a hand around a pole. Any movement of this domain is therefore transmitted to the ion-binding site, changing the local chemical environment of proton-binding side chains, and vice versa. In bacteriorhodopsin, small movements of proton-binding side chains cause shifts in their pK_a (where K_a is the acid dissociation constant), resulting in proton pumping (8–10). We propose that the proton-binding residues in the H⁺-ATPase—particularly Arg⁶⁹⁵ and His⁷⁰¹ on M5, as well as Asp⁷³⁰ and Glu⁸⁰⁵—undergo similar pK_a changes due to a change in their local environment, resulting in the release of bound protons to the outside.

The autoinhibitory COOH-terminal extension of the H⁺-ATPase contains a regulatory site at Ser⁹¹³ and Thr⁹¹⁴ (16–18), phosphorylated by a specific kinase (19). A yeast double mutant of these residues locks the enzyme in the

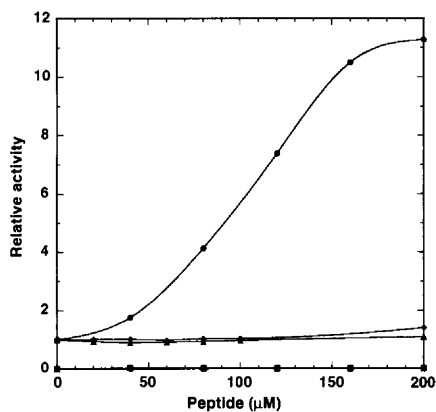
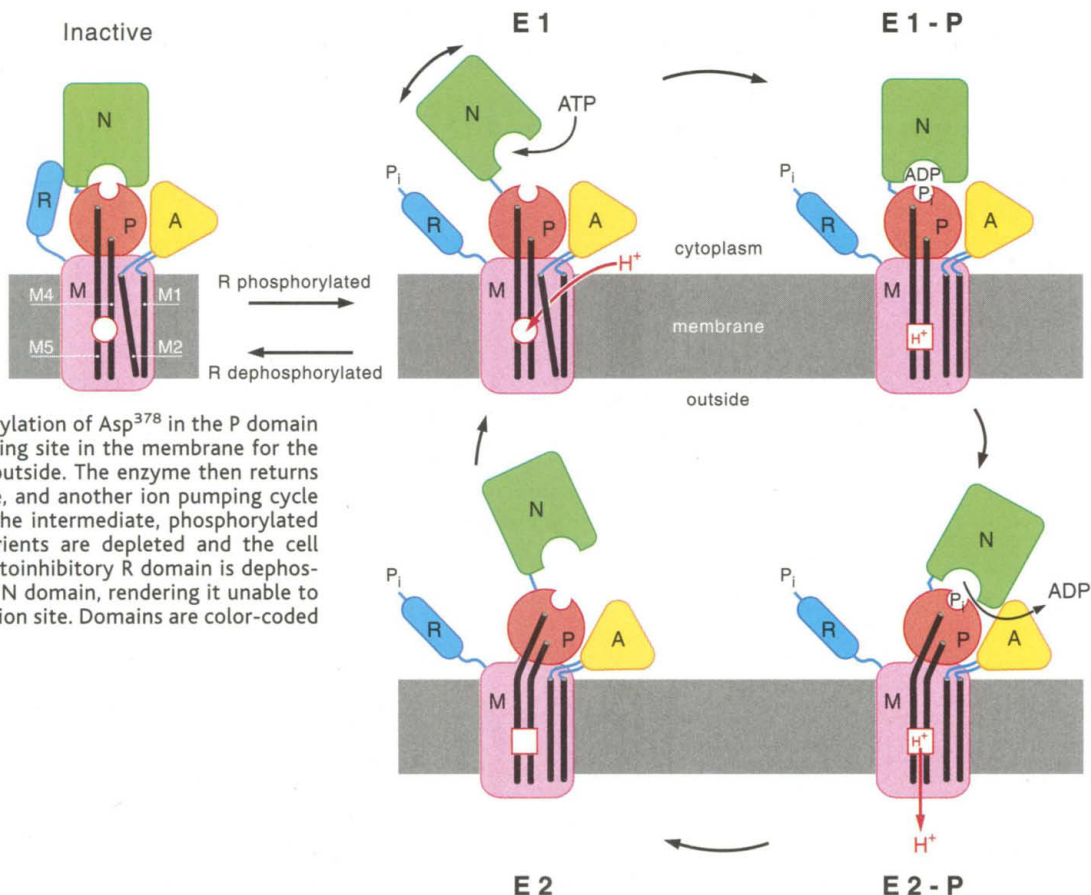


Fig. 3. Stimulation of ATPase activity by the regulatory R domain. A peptide of the 38 COOH-terminal residues of the *Neurospora* proton ATPase was added to a standard ATPase assay (24). At peptide concentrations of 200 μ M and above, ATPase activity (circles) increased by more than a factor of 10 relative to the activity in the absence of added peptide. Maximum stimulation was observed at pH 6.8. Control peptides of similar size (diamonds, thiocalcitonin; triangles, insulin chain B) had no effect. The peptide itself (squares) had no ATPase activity.

Fig. 4. Proposed mechanism of proton transport and regulation. The proton pump is activated by reversible phosphorylation of the regulatory R domain. In the open E1 state of the H⁺-ATPase, protons have access to the proton-binding site in the M domain. Proton binding causes a conformational change that is transmitted via M4 and M5 to the P and A domains, causing them to reorient. The A domain movement pulls M2 into a position that blocks the proton path to the binding site in the membrane. Phosphorylation of Asp³⁷⁸ in the P domain reduces the affinity of the binding site in the membrane for the proton that is released to the outside. The enzyme then returns to the E1 state via the E2 state, and another ion pumping cycle starts. E1-P and E2-P refer to the intermediate, phosphorylated states of the enzyme. As nutrients are depleted and the cell metabolism shuts down, the autoinhibitory R domain is dephosphorylated and attaches to the N domain, rendering it unable to deliver ATP to the phosphorylation site. Domains are color-coded as in Figs. 1 and 2.



inactive state, whereas deletion of the autoinhibitory extension results in constitutive activation (16–18). The fit of the four principal domains and the NH₂-terminal extension left one small but prominent part of the H⁺-ATPase map unoccupied to accommodate the COOH-terminal extension. This part of the map, located above the cytoplasmic end of M10 (fig. S2D), had roughly the shape and size of a membrane-spanning helix. We therefore modeled residues 884 to 920 as a predominantly α-helical structure (cyan in Fig. 1) with kinks at Pro⁸⁹³, and at Ser⁹¹³ and Thr⁹¹⁴ to fit the map, and linked it to M10 by a stretch of extended chain. The well-defined shape and its position in the H⁺-ATPase hexamer (fig. S3) indicate that it must be regarded as a separate domain. In accordance with its function, it is termed the regulatory (R) domain. The R domain fit puts Ser⁹¹³/Thr⁹¹⁴ next to the N and P domains. This is consistent with numerous second-site revertants (7), which require a physical interaction of these residues with the main body of the enzyme.

We investigated the effect of the R domain on the activity of the *Neurospora* plasma membrane H⁺-ATPase with a synthetic peptide of the 38 COOH-terminal residues. Addition of this peptide stimulated the ATPase activity by as much as a factor of 10, depending on pH (Fig. 3), whereas other peptides of similar size had no effect. This suggests that the R domain exerts its regulatory function by attaching to the N domain, restricting its mobility by tethering it to the membrane. We hypothesize that the R domain is released upon phosphorylation, leaving the N domain free to move and able to deliver ATP to the P domain. An excess of R domain peptide would have the same effect, replacing the enzyme's own R domain in the binding site and thus enabling the hinge movement of the N domain. The resulting proposed mechanism of proton pumping and enzyme regulation is shown in Fig. 4.

The H⁺-ATPase model indicates that the R domain interacts with the next-door monomer at Gln⁶²⁴ and Arg⁶²⁵ in helix 5 of the P domain. The arginine is completely conserved in the hexamer-forming fungal H⁺-ATPases, which suggests that the R domain links adjacent monomers and thus has a critical role in hexamer formation. Characteristic crystalline patches of rosette-shaped particles are common in freeze-fracture replicas of starving yeast (20) and *Neurospora* cells (21). The arrays have the same unit cell parameters and morphology as single-layer two-dimensional crystals of the *Neurospora* H⁺-ATPase (22). We conclude that the H⁺-ATPase hexamers are a storage form of the inactive enzyme. The minor domain movements observed in low-resolution maps of isolated ATPase hexamers in the presence and absence of ADP (23) are unlikely to reflect the well-documented large conformational changes in fully active P-type ATPases.

The striking structural similarity be-

tween the H⁺-ATPase and the distantly related Ca²⁺-ATPase implies that all other P-type ATPases—including the Na⁺,K⁺-ATPase, the H⁺,K⁺-ATPase, and the heavy metal pumps—have essentially similar structures and can be modeled on the Ca²⁺-ATPase. The reason for this remarkable conservation of structural detail must be strong evolutionary pressure to maintain the functional sites of each domain in their exact spatial relationship for efficient ion pumping.

References and Notes

1. J. V. Møller, B. Juul, M. le Maire, *Biochim. Biophys. Acta* **1286**, 1 (1996).
2. D. J. Bigelow, G. Inesi, *Biochim. Biophys. Acta* **1113**, 323 (1992).
3. E. Goormaghtigh, L. Vigneron, G. A. Scarborough, J.-M. Ruyschaert, *J. Biol. Chem.* **269**, 27409 (1994).
4. C. Toyoshima, M. Nakasako, H. Nomura, H. Ogawa, *Nature* **405**, 647 (2000).
5. P. Zhang, C. Toyoshima, K. Yonekura, N. M. Green, D. L. Stokes, *Nature* **392**, 835 (1998).
6. M. Auer, G. A. Scarborough, W. Kühlbrandt, *Nature* **392**, 840 (1998).
7. P. Morsomme, C. W. Slayman, A. Goffeau, *Biochim. Biophys. Acta* **1469**, 133 (2000).
8. J. Tittor, D. Oesterhelt, E. Bamberg, *Biophys. Chem.* **56**, 153 (1995).
9. C. Zscherp, R. Schlesinger, J. Tittor, D. Oesterhelt, J. Heberle, *Proc. Natl. Acad. Sci. U.S.A.* **96**, 5498 (1999).
10. H. Luecke, *Biochim. Biophys. Acta* **1460**, 133 (2000).
11. C. Xu, W. J. Rice, W. He, D. L. Stokes, *J. Mol. Biol.* **316**, 201 (2002).

12. M. V. Ponomarev, W. A. Cramer, *Biochemistry* **37**, 17199 (1998).
13. C. R. Lancaster, H. Michel, *Structure* **5**, 1339 (1997).
14. G. Hummer, J. C. Rasaiah, J. P. Noworyta, *Nature* **414**, 188 (2001).
15. S. Lutsenko, K. Petrukhin, M. J. Cooper, C. T. Gilliam, J. H. Kaplan, *J. Biol. Chem.* **272**, 18939 (1997).
16. F. Portillo, P. Eraso, R. Serrano, *FEBS Lett.* **287**, 71 (1991).
17. R. Serrano, F. Portillo, B. C. Monk, M. G. Palmgren, *Acta Physiol. Scand. Suppl.* **607**, 131 (1992).
18. F. Portillo, *Biochim. Biophys. Acta* **1469**, 31 (1999).
19. A. Goossens, N. De La Fuente, J. Forment, R. Serrano, F. Portillo, *Mol. Cell. Biol.* **20**, 7654 (2000).
20. O. Kübler, H. Gross, H. Moor, *Ultramicroscopy* **3**, 161 (1978).
21. W. Kühlbrandt, J. Dietrich, W. Haase, unpublished data.
22. M. Cyrklaff, M. Auer, W. Kühlbrandt, G. A. Scarborough, *EMBO J.* **14**, 1854 (1995).
23. K. H. Rhee, G. A. Scarborough, R. Henderson, *EMBO J.* **21**, 3582 (2002).
24. J. P. Hennessey, G. A. Scarborough, *J. Biol. Chem.* **263**, 3123 (1988).
25. We thank W. Haase for performing the freeze-fracture electron microscopy, and D. Stokes and M. Palmgren for discussion. The model coordinates have been deposited in the Protein Data Bank (accession code 1MHS).

Supporting Online Material

www.sciencemag.org/cgi/content/full/1072574/DC1
 Methods
 Figs. S1 to S3
 Table S1
 References

5 April 2002; accepted 25 July 2002
 Published online 8 August 2002;
 10.1126/science.1072574
 Include this information when citing this paper.

Nitrogenase MoFe-Protein at 1.16 Å Resolution: A Central Ligand in the FeMo-Cofactor

Oliver Einsle,^{1,2} F. Akif Tezcan,² Susana L. A. Andrade,^{1,2}
 Benedikt Schmid,² Mika Yoshida,^{1,2} James B. Howard,³
 Douglas C. Rees^{1,2*}

A high-resolution crystallographic analysis of the nitrogenase MoFe-protein reveals a previously unrecognized ligand coordinated to six iron atoms in the center of the catalytically essential FeMo-cofactor. The electron density for this ligand is masked in structures with resolutions lower than 1.55 angstroms, owing to Fourier series termination ripples from the surrounding iron and sulfur atoms in the cofactor. The central atom completes an approximate tetrahedral coordination for the six iron atoms, instead of the trigonal coordination proposed on the basis of lower resolution structures. The crystallographic refinement at 1.16 angstrom resolution is consistent with this newly detected component being a light element, most plausibly nitrogen. The presence of a nitrogen atom in the cofactor would have important implications for the mechanism of dinitrogen reduction by nitrogenase.

Biological nitrogen fixation provides the dominant route for the transformation of atmospheric dinitrogen into a bioavailable form, ammonia (1–4). This process is catalyzed by the enzyme nitrogenase, which consists of two component metalloproteins, the Fe-protein and the MoFe-protein. The

homodimeric Fe-protein couples adenosine 5'-triphosphate hydrolysis to interprotein electron transfer and is the only known mechanistically competent source of electrons for the catalytically active component, the MoFe-protein. The latter is organized as an α₂β₂ tetramer that contains two